# An experimental study on gravity waves through a floating viscoelastic cover

Sree, Dharma K. K.; Law, Adrian Wing-Keung; Shen, Hayley H.

2018

Sree, D. K. K., Law, A. W.-K., & Shen, H. H. (2018). An experimental study on gravity waves through a floating viscoelastic cover. Cold Regions Science and Technology, 155, 289-299. doi:10.1016/j.coldregions.2018.08.013

https://hdl.handle.net/10356/137039

https://doi.org/10.1016/j.coldregions.2018.08.013

# AN EXPERIMENTAL STUDY ON GRAVITY WAVES THROUGH A FLOATING VISCOELASTIC COVER

Dharma Sree K. K. [1,2], Adrian Wing-Keung Law[1,2*], Hayley H. Shen[1,3]

[1]Environmental Process Modelling Centre (EPMC), Nanyang Environment and Water Research Institute (NEWRI), Nanyang Technological University, 1 CleanTech Loop, CleanTech One, #06-08, Singapore 637141

[2]School of Civil and Environmental Engineering, Nanyang Technological University, N1-01a-29, 50 Nanyang Avenue, Singapore 639798

[3]132 Rowley Laboratories, Civil and Environmental Engineering, Clarkson University, Potsdam, NY, USA 13699-5710

[*] Corresponding author. Phone number: +65 67905296

Email address: cwklaw@ntu.edu.sg (A.W.K Law)

**ABSTRACT**

We report the results of a laboratory study conducted to investigate the dispersion relation and attenuation of surface waves under viscoelastic floating covers. The study uses oil-doped polydimethylsiloxane (PDMS) with different viscoelastic properties quantified in-situ using a rheometer. An additional test is made with a floating PVC film to estimate possible attenuation in the boundary layer under the cover. Within the frequency range tested, the wavelength deviates from open water case negligibly under the PVC film. But for the PDMS covers, depending on the material property, cover thickness and incident wave period, both wave lengthening and shortening are observed. With thin PDMS covers, the measured wavelength matches well with three theoretical predictions based on different viscoelastic rheological models, while the thick cover shows some discrepancy especially for shorter wave periods. In terms of wave attenuation, however, large discrepancies are observed between the measured data and theoretically predicted results for all PDMS covers. Various mechanisms that could contribute to the discrepancies are considered. The most important mechanism is the boundary layer effect, as demonstrated by the measured wave attenuation from the PVC film. The overall results indicate that the attenuation due to the oscillatory boundary layer underneath the floating cover, which has not been included in the viscoelastic theories, contributes significantly to the discrepancies. Direct measurement of the fluid flow under a periodically flexing cover and the related attenuation rate is a challenging but highly important future study.

Keywords: viscoelastic; floating covers; PDMS; wave dispersion; attenuation.

## 1. Introduction

Arctic ice reduction has created longer fetches, which aid in the generation of larger gravity waves that could penetrate hundreds of kilometers of distance through ice covers. With increased interests in Arctic shipping (Smith and Stephenson, 2013), better knowledge of the wave climate in the Marginal Ice Zone (MIZ) is required to facilitate navigation near the ice edge. Thus, there is an appreciable demand to understand wave propagation through diverse types of ice covers in the MIZ (the glossary and associated ice cover images can be found at http://aspect.antarctica.gov.au/home/conducting-sea-ice-observations).

Field studies based on observations from satellites (Wadhams et al., 2002) and in-situ measurements (Wadhams et al., 1986, 1988; Meylan et al., 2014) showed that ice covers behave primarily as a low-pass filter, which scatters and attenuates the high frequency wave components. Satellite observations also suggested changes of wavelength and thus the speed of energy propagation (Schulz-Stellenfleth and Lehner, 2002), dispersion relations in ice fields have been observed in field experiments conducted by Fox and Haskell (2001) and Sutherland and Rabault (2016). To determine the wave propagation under diverse types of ice covers from first principles is a challenging task. Therefore, various theories have been proposed based on different assumptions.

The initial theoretical attempts on wave propagation through a viscous medium were done independently by Stokes (1851) and Lamb (1932) for an infinite deep single layer with constant

viscosity. The first two-layer viscous model was developed by Weber (1987) assuming ice as a thin viscous layer over infinitely deep inviscid water. This was later extended to inviscid finite deep water by Keller (1989), in which the momentum equation of the floating high viscous layer was coupled with that of the inviscid layer underneath to solve for the dispersion relation. Newyear and Martin (1999) used this theory to inversely determine the viscosity of grease ice. De Carolis and Desiderio (2002) and De Carolis et al. (2005) later extended the Keller's model to include the viscosity of water under ice covers.

In addition to the two-layer viscous model (Keller, 1998), two other classical theories that describe wave dispersion through an idealized floating cover are of particulate relevance here. The first theory assumes the large unbroken ice cover as a thin elastic plate (Greenhill, 1886). This theory demonstrates the changes of wavelength, but it does not allow wave attenuation. The second theory, the mass loading model, assumes the ice cover as a surface composed of non-interacting mass points (Peters, 1950; Weitz and Keller, 1950; Keller and Weitz, 1953). This theory is later pointed out to be a special case of the thin elastic plate theory when the elasticity is set to zero (Squire, 1993). The mass loading theory predicts only wave shortening and no attenuation. Among these three theories, only two-layer viscous model predicts attenuation.

Each of the three classical theories partially captures the mechanical processes associated with an ice cover that moves and deforms in a wave field. The thin elastic theory focuses on the elastic strain as well as the inertia of the ice cover, the mass loading theory considers only the inertia, and the viscous theory includes the strain-rate-dependent dissipation. Recognizing that all these

processes may co-exist, several viscoelastic theories have been proposed to model sea ice in a wave field. Squire and Allan (1980) extended the thin elastic plate theory by introducing a complex elasticity. Wang and Shen (2010) extended the model by Keller (1998) to consider the ice cover as a Voigt-type viscoelastic continuum. This continuum model was based on the concept that in any representative region of an ice cover, part of it would experience elastic deformation while the rest would undergo some rate dependent dissipation. The resulting dispersion relation was shown to converge under proper limiting conditions to all three classical theories mentioned above. In addition to these two viscoelastic theories, Mosig et al. (2015) investigated another relevant theory developed for wind-induced vibration of floating roofs on oil storage tanks (Robinson and Palmer, 1990). The fundamental principles of this theory are analogous to the existing models on sea ice.

A viscoelastic dispersion relation is appealing for wave modelling in MIZ, because it can predict different wavelength changes and wave energy attenuation by choosing different combinations of elastic and viscous parameters. By fitting the observational data obtained from different ice cover types, it is envisioned that one may connect different ice types to their distinct viscoelastic properties, as demonstrated in the laboratory studies (Newyear and Martin, 1999; Zhao and Shen, 2015) and a field study (Cheng et al., 2017). In Zhao and Shen (2015), experimental data were used to calibrate the viscoelastic parameters for different ice covers. However, a direct validation of the viscoelastic model by Wang and Shen (2010) has not been done. However, the validity of the dispersion relation from these viscoelastic theories needs to be established in order to confidently apply it to the field. Such model validation can only be done in the laboratory under controlled conditions with true viscoelastic materials and clean wave forcing. In real ice conditions, other than the rheological properties of sea ice, bottom roughness of floating ice floes

(Kohout et al, 2011), ice pack compression (Liu and Mollo Christensen, 1988) etc. could also contribute to wave damping, though they are not considered in the above-mentioned continuum models. Laboratory experiments, closer to theoretical conditions with less complexities, thus enable the comparison of the experimental results with different viscoelastic theories to validate the existing theories and point out missing mechanisms. In addition to enhancing our understanding of wave propagation through ice covers, the finding from the present study is also relevant to the wave interactions with very large floating structures (Hermans, 2004).

We performed the first attempt of experimental validation of viscoelastic theories in Sree et al. (2016a). A set of laboratory experiments were conducted using viscoelastic covers with different properties, which were measured in-situ in the laboratory using a rotational rheometer. The covers were made of oil-doped polydimethylsiloxane (PDMS). Different properties were achieved by varying the percentage of a curing agent added during preparation. The model predictions by Wang and Shen (2010) were found to be generally consistent with the experimental data from wave flume experiments, both in terms of the switching of normalized wavelength from less than to greater than 1, as well as the magnitude of the change. Thus, the study provided a general confirmation of the viscoelastic theory by Wang and Shen (2010) in terms of the dispersion relation with respect to the viscoelastic properties and wave characteristics. However, there were uncertainties introduced by the free-body motion of the floating cover due to its finite extent. In addition, it was not possible to examine the wave attenuation through the viscoelastic cover because the magnitude of wave decay through the cover was relatively insignificant compared to the above-mentioned uncertainties.

In the current study, we continued the laboratory validation effort of Sree et al. (2016a) using the viscoelastic PDMS material with a much longer cover length as well as different cover thicknesses. The additional combinations of viscoelastic cover properties and wave characteristics used in the new experiments provide more data for further confirmation of the dispersion relation predicted from viscoelastic theories. Furthermore, experimental measurements on wave attenuation through a true viscoelastic cover are also reported for the first time, which enables the close examination of another aspect of predictions of critical importance from viscoelastic theories.

In the following sections, we will begin by describing the three theoretical models: Squire and Allan (1980), Robinson and Palmer (1990), Wang and Shen (2010). It is followed by material preparation along with its mechanical properties and the experimental setup for wave experiments. Data analysis for wave celerity (phase speed) and attenuation, as well as comparison of the experimental results with theoretical models are presented, followed by the discussion and conclusions.

## 2. Viscoelastic Models for Sea Ice

The three existing viscoelastic theories to be considered in this study are: Squire and Allan (1980), Robinson and Palmer (1990), and Wang and Shen (2010), which are abbreviated as SA, RP and WS models respectively in the following sections. A brief description of these three theories is given below. The configuration of all three models is a two-layer system with the upper layer as a viscoelastic cover (representing floating sea ice) with thickness $h$, and density $\rho_1$. The lower layer

147 represents inviscid water with depth $H$ and density $\rho_2$. In each case, a relation between the wave
148 frequency and the complex wave number, $k = k_s + ik_i$ is given, where $k_s$ is the real wavenumber
149 related to the celerity / phase speed and $k_i$ is the attenuation coefficient. In all three models,
150 exponential decay is a natural consequence of the complex wave number from the dispersion
151 relation.

152

153 Squire and Allan (1980) assumed the two-layer system as a thin plate over deep water, with the
154 top layer modelled as a linear Maxwell-Voigt model with four model parameters. For the present
155 case, the system is simplified with a Voigt model and modified with a finite water depth. The Voigt
156 model has two parameters defined by the complex shear modulus, $G_V = G - i\sigma\rho_1\nu$, where $G$ is the
157 shear modulus, $\nu$ is the kinematic viscosity and $\sigma$ is the wave angular frequency. The dispersion
158 relation is obtained as (Li et al., 2015)

159 $$\left(\sigma^2 - Q_{SA} g k \tanh kH\right) = 0 \quad (1)$$

160 $$Q_{SA} = \frac{G_V h^3}{6g\rho_2(1-\vartheta)}k^4 - \frac{\rho_1 h\sigma^2}{\rho_2 g} + 1 \quad (2)$$

161 where, $g$ is the acceleration due to gravity and $\vartheta$ is the Poisson's ratio.

162

163 Robinson and Palmer (1990) assumed that the top cover is a purely elastic Euler Bernoulli beam.
164 They added a damping/viscous term proportional to the velocity of the vertical displacement under
165 wave action (Mosig et al., 2015). The dispersion relation for their model is

166 $$\left(\sigma^2 - Q_{RP} g k \tanh kH\right) = 0 \quad (3)$$

167 $$Q_{RP}= \frac{Gh^3}{6g\rho_2(1-\vartheta)}k^4 - \frac{\rho_1 h\sigma^2}{\rho_2 g} + 1 - \frac{i\sigma}{\rho_2 g}\gamma \quad (4)$$

168 Unlike the SA model, where the viscosity is considered a material property, the viscous term $\gamma$
169 here is admitted as purely phenomenological, which must be determined by fitting the attenuation
170 to match with the experimental results.

171

172 Wang and Shen (2010) assumed that the upper layer is a viscoelastic fluid of the Voigt type. The
173 dispersion relation is

174 $$\left(\sigma^2 - Q_{WS}gk\tanh kH\right)J = 0 \quad (5)$$

175 with

176 $$Q_{WS} = 1 + \frac{\rho_1 g^2 k^2 S_k S_\alpha - \left(N^4 + 16k^6 {\alpha_k}^2 \nu_e^4\right) S_k S_\alpha - 8k^3 \alpha_k \nu_e^2 N^2 (C_k C_\alpha - 1)}{J} \quad (6)$$

177 and

178 $$J = gk(4k^3 \alpha_k \nu_e^2 S_k C_\alpha + N^2 C_k S_\alpha - gk S_k S_\alpha) \quad (7)$$

179 where $\nu_e = \nu + iG/\rho_1\sigma$is the complex viscosity, $\alpha_k = k^2 - i\sigma/\nu_e$,$S_k = \sinh(kh)$, $S_\alpha = \sinh(\alpha_k h)$, $C_k$
180 $= \cosh(kh)$, $C_\alpha = \cosh(\alpha_k h)$ and $N = \sigma + 2ik^2\nu_e$. As shown in Wang and Shen (2010) and
181 Mosig et al. (2015), this dispersion relation has multiple roots. The nature of these roots has been
182 discussed in detail in Zhao et al. (2017). The dominant root, i.e. the one corresponding to the
183 gravity wave mode, is selected in the present study.

184

For the present experiments, two types of floating covers were used: PVC film and PDMS covers. The thickness of the viscoelastic PDMS layer $h$ was either 0.01 m or 0.02 m, density $\rho_1 = 940$ kg/m$^3$, water depth $H =$ 0.3 m and water density $\rho_2 = 1000$ kg/m$^3$. The determination of viscosity and shear modulus for the PDMS covers will be discussed in Section 3.2. These values of material properties will be used to derive the theoretical wave speed and attenuation from SA and WS models. The thickness of the PVC film was on the order of $10^{-4}$ m. Its mechanical properties were not directly measured. As will be discussed later, for such thin film its mechanical properties become irrelevant for the SA and WS models. The RP model requires a phenomenological parameter which can only be calibrated.

## 3. Experiments

### 3.1 Material preparation

In the present study, the viscoelastic covers are 3 m long, which span from the center of the flume to the beach. Wave experiments using 1 m long covers had been reported in Sree et al. (2016a) earlier, which assessed the dispersion relation under the viscoelastic cover and the results were found to agree well with the predictions by the WS model. However, the 1 m cover length did not allow the determination of wave attenuation since the damping was too slight to be accurately measured.

206 The floating viscoelastic covers for the present experiments are made of PDMS which is identical
207 to Sree et al. (2016a). The elastomer consists of a silicone oil base and curing agent/ cross linker,
208 which is commercially available as Sylgard 184 Silicone Elastomer kit. The preparation of the
209 PDMS covers involves three main steps: mixing the components (base, curing agent and white
210 oil), degassing and natural curing. Sree et al. (2016a) described the novel development of the
211 natural curing approach (as opposed to the elevated temperature approach for previous applications
212 in the literature) for the preparation of viscoelastic floating layers in wave experiments as well as
213 the detailed procedures using a curing tray**.**

214

215 The greatest challenge in the current experiments is the natural curing of the 3 m long covers. The
216 process of transferring a long and soft PDMS cover prepared outside the wave flume in the curing
217 tray, as used in the previous study (Sree et al. 2016a), often damages the cover. We thus developed
218 another new set of in-situ procedures to make the cover inside the wave flume as described in Sree
219 et al. (2016b).

220

221 Covers with various levels of viscoelasticity are produced by varying the percentage of curing
222 agent used ($m_{CA} =$ 4, 6, 8 and 10%), where $m_{CA} = \frac{M_{CA}}{M_{CA} + M_B}$, $M_{CA}$ and $M_B$ represent the mass of
223 curing agent and base respectively. The freshly prepared PDMS material is left to cure for 7 days
224 at room temperature. Fig. 1 shows the cover inside the flume under curing. The inside walls of the
225 3 m long confined region for the PDMS cover to cure are lined with transparent plastic films to
226 prevent the adhesion of the PDMS cover to the flume. The layer thickness is $h_s =$ 0.01 m for

227 covers with $m_{CA} =$ 6, 8, and 10%. For the 4% mass of curing agent, two thicknesses, $h_s =$ 0.01
228 m and 0.02 m, are used.

229 **<Fig. 1>**

230 3.2 Material testing

231

232 The rheological properties of oil-doped PDMS covers are analyzed once the covers become stable
233 after curing. The storage modulus, $G^{'}$ and the loss modulus $G^{''}$ are determined using small
234 amplitude oscillatory shear tests in a rheometer (Anton Paar, MCR 302, Germany), with a parallel
235 plate geometry. A detailed discussion about the two categories of rheometer testing a) amplitude
236 sweep and b) frequency sweep, is provided in Sree et al. (2016a). Three samples are tested for each
237 cover with the specific $m_{CA}$ to confirm the repeatability of results. The stability in the rheological
238 properties is confirmed for a period of two weeks after the material is fully cured, hence the wave
239 experiments are performed within this stable period.

240

241 The range of angular frequency ($\omega$) used for the rheometric testing is set equal to the angular
242 frequencies ($\sigma$) of the wave tests. The test results are shown in Table 1. When $m_{CA}$ is increased
243 from 4 to 10 %, the material becomes stiffer with larger $G^{'}$ but smaller $G^{''}/G^{'}$. The values obtained
244 for $G^{'}$ and $G^{''}$ shows that the PDMS material properties can be approximated by the Voigt model
245 with $G^{'}$ nearly constant and $G^{''}$ monotonically increasing with frequency (Sree et al. 2016a). The
246 viscoelastic parameters used in the SA and WS models are related to the storage and loss modulus
247 as $G = G'$, $\nu = G^{''}/\rho_1\sigma$. Table 1 shows that viscosity increased with $m_{CA}$. The Poisson's ratio is
248 not measured; we use the value $\vartheta = 0.5$ for PDMS neglecting the influence of oil in the property

(Folch, 2012). The irrelevance of finite mechanical properties for PVC film in this study will be discussed in Section 5.2.4. Instead the PVC film experiments are performed to estimate the influence of factors other than the rheological properties of a cover on surface waves, i.e. the boundary layer dissipation under a floating cover.

**<Table 1>**

### 3.3 Wave flume experimental setup

The laboratory experiments are conducted in a wave flume (see Fig. 2) at the Environmental Process Modelling Centre (EPMC) Laboratory of Nanyang Environment and Water Resources Institute, Singapore. The wave flume, with [length $L$, width $B$, depth $D$] = [8, 0.3, 1] m, is made of tempered transparent glass panels and is filled with fresh water up to a height, $d$ = 0.3 m. It is equipped with a piston-type wave generator at one end and an inclined mesh type wave absorber beach (slope angle = 38$^o$) at the other end (see Fig. 2). The wave generator can produce regular waves as well as irregular waves, however only regular waves are considered in this study.

**<Fig. 2>**

Monochromatic waves with periods from $T$ = 0.5 to 1.0 s at 0.05 s intervals are generated for the experiments. A static calibrated capacitance wave gauge is installed near the wave generator to control the stroke of the piston to produce incident waves of the required amplitude. The values of wave steepness ($k_o a$) for the experiments are summarized in Table 2, where $k_o$ is the wavenumber and $a$ is the wave amplitude in open water. Smaller amplitudes are used for high frequency cases, to prevent the water running over the cover, referred to as overwash at the leading edge.

We note that for the range of waves tested, the effect of surface tension of water, $T_s$, on the dispersion relations can be neglected as $\frac{T_s k^2}{\rho g} \sim 0.002 \ll 1$.

**<Table 2>**

In the present study, the 3-m long PDMS covers extend up to the beach. Hence, the beach and the inertia for the long covers together minimize the possible surge or drift as well as free-body rotation. Seven ultrasound sensors (US325, Ultra lab 40D, General Acoustics, Germany) with resolution of 0.18 mm and sampling frequency of 50 Hz are installed above the floating covers to record its surface deflection upon wave action. The synchronized data from all ultrasound sensors are then collected from LABVIEW, using a common data acquisition system (NI 9215, National Instruments, Texas). The first ultrasound sensor is held 20 cm away from the leading edge to avoid possible edge effects like flapping due to damped travelling waves. The positioning of ultrasound sensors over the viscoelastic sheets are provided in Appendix A. The repeatability of the experiments is checked by performing each experiment at least three times (see Fig. 3). To increase the time resolution of the ultrasound sensor records, prior to data analysis, numerical interpolation with the $PCHIP$ function (Piecewise Cubic Hermite Interpolating Polynomial) is used to increase the data rate from 50 Hz to 200 Hz. Only the first three fully developed waves are considered in the analysis (see Fig. 3) instead of continuous wave train to avoid the effect of reflection from the beach which can excite partially standing waves inside the wave flume.

**<Fig.3 >**

## 4. Data Analysis and Results

### 4.1 Wave celerity

Wavenumbers are calculated in the same way as described in Sree et al. (2016a) for the 1 m long PDMS covers. Since only three waves are involved in the data analysis, the spectral method cannot be used properly to determine the wave celerity. Instead, the celerity is determined by measuring the time corresponding to the peaks of the three waves with the $findpeaks$ function at each sensor. The time differences between the corresponding crests of the first ultrasound sensor US1 and the other sensors USi, i from 2 to 7, are then calculated. The celerity is calculated as

$$c_s = \frac{\Delta x_i}{\Delta t_i} = \frac{\sigma}{k_s} \tag{8}$$

where, $\Delta x_i$ is the distance of the $i^{\text{th}}$ ultrasound sensor USi from US1, and $\Delta t_i$ is the mean of the corresponding time lapse taken for the wave crest to travel between the two sensors considered, and $k_s$ is the wavenumber under the floating covers.

For the PVC film cover, ${c_s}/{c_o} \approx 0.99 - 1.01$ for all wave periods tested. Hence, the resulting dispersion relation is unchanged from the open water condition. For the PDMS covers, the measured celerity behaves almost the same as with the 1 m case (Sree et al., 2016a). As shown in Fig. 4, $c_s$ along the covers is different from the open water celerity, $c_o$. For $T$ = 0.5 s, $c_s < c_o$ for $m_{CA}$= 4%. It increases with increasing $m_{CA}$ and finally becomes greater than $c_o$. The increase of celerity with increasing $m_{CA}$ is less dramatic with increasing wave period. The celerity obtained using the sensors near the free edges shows deviation from the values obtained away from the edges, which can be attributed to the edge effect from the damped travelling waves (Fox and

312 Squire, 1990). For the 1 m cover studied in Sree et al. (2016a), the proportion of the data affected
313 by the edge was greater.

314 **< Fig. 4>**

315 4.2 Wave attenuation along viscoelastic covers

316

317 The vertical locations of crests and troughs from the interpolated data (200 Hz) are determined
318 using the *findpeaks* function. The wave height is then obtained as the distance between the adjacent
319 crest and trough. The wave amplitude, $A_x$, calculated as half of the wave height, is plotted against
320 the distance along the cover as shown in Fig. 5. For wave amplitude measurements, especially at
321 small amplitudes in our study, sensor resolution is an important issue. With the sensor resolution
322 at ~ 0.18 mm, less than 10% of the minimum amplitude shown in Fig. 5, the data are adequate for
323 our attenuation analysis.

324

325 To compare with the three viscoelastic theories, we fit the measured amplitude data with an
326 exponential curve, as shown in Fig. 5. The attenuation coefficient for each case is defined as the
327 parameter, $\alpha$, of the fitting curve

328 $$A_x = A_o e^{-\alpha x} \quad (9)$$

329 where, $A_x$ is the wave amplitude at the distance $x$ from the leading edge and $A_o$ is the amplitude at
330 $x = 0$. From Fig. 5, the wave amplitude clearly decreases with distance from the leading edge for
331 $T = 0.5$ s. The dependence of attenuation coefficient on both the wave period and thickness of the

cover are clearly visible. The root mean square error for the fitted curve is confirmed to be less than $10^{-4}$ m for all the test cases.

**< Fig. 5>**

## 5. Results and discussions

### 5.1 Wavenumber

The variation of normalized wavenumber, $\kappa = k_s/k_o$ with wave period is provided in Fig. 6. In this figure and all subsequent figures, the theoretical curves are from Equations 1, 3 and 5 for the three models considered in Section 2. The required elastic parameters for all the three models and the viscous parameters for the SA and WS models are from Table 1. For the RP model, however, the viscous parameter is inversely calculated by fitting the attenuation data for one case ($T = 0.55$ s for $m_{CA} = 4\%$) with the theoretical model. This value is then applied for all other cases to calculate the real and imaginary parts of the complex wavenumber, $k$. The experimental results with the 1 m PDMS cover reported in Sree et al. (2016a) is also superimposed in Fig. 6. With the longer PDMS covers and lesser edge effects, the measured wavelength compares even better with the theoretical predictions from the WS model than Sree et al. (2016a). There is practically no difference between the three predictions within the tested parameter range.

For open water, $\kappa = 1$; wave lengthening compared to open water case is represented by $\kappa < 1$ and wave shortening by $\kappa > 1$. The normalized wavenumber depends on both the material

354 characteristics and wave period. For $h_s$= 0.01 m, all three viscoelastic models predict the
355 experimental results well. Fig. 6 shows that with $m_{CA}$ = 4% and thickness, $h_s$ = 0.01 m, wave
356 shortening occurs for all wave periods. However, the behavior of $\kappa$ is not monotonic. The
357 dimensionless wavenumber increases from $T$ = 0.5 s to 0.6 s to reach the maximum then drops
358 with further increase of $T$. With $m_{CA}$ = 6%, the wavenumber is similar to the open water case for
359 $T$ = 0.5 s. When the wave period is increased, an increase in $\kappa$ followed by a decrease is again
360 seen. With $m_{CA}$ = 8 and 10 %, wave lengthening is observed for $T$ = 0.5 s, while all other cases
361 show wave shortening. This non-monotonic change of wavenumber with wave period is shown in
362 all three viscoelastic models and the experimental data. Hence, the modification of wavenumber
363 in a covered region, with respect to open water case, depends largely on the combination of wave
364 period and the material characteristics of the covers. This non-monotonic behavior was mentioned
365 in the theoretical studies by Squire (1993) and Collins et al. (2017). However, for the thicker
366 PDMS cover ($h_s$= 0.02 m), unlike the thinner covers with the same $m_{CA}$ = 4%, differences between
367 all three theoretical predictions and experimental data are noted. Additional discussion on this
368 wave number discrepancy is provided in the following sections.

369 **<Fig. 6>**

370

371 5.2 Wave attenuation

372

373 A comparison of the attenuation coefficient, $\alpha$, obtained from the experiments (circles) and the
374 imaginary part of the complex wavenumber, $k_i$, obtained from the theories (lines) are shown in
375 Fig. 7. The error bars showed the 95% confidence bound for the coefficient obtained when fitting

the experimental data for average amplitude of the three fully developed waves with an exponential curve. Qualitatively, the attenuation coefficient decreases with increasing wave period, except with $m_{CA}$ = 10% and the thicker sheet with $m_{CA}$ = 4%, where a rollover is seen. This rollover phenomenon is not predicted by two of the three theoretical models; only the RP model demonstrates a mild rollover for larger $m_{CA}$ or a thicker cover. Quantitatively, except with the RP model, a significant difference between the experimental results and the theoretical predictions is observed. As explained earlier, unlike the other two models where the viscous parameter is from the actual rheometer data, the empirical viscous parameter, $\gamma$ for RP model is calibrated from data fitting. A good comparison between RP model and the experimental data is thus expected.

**<Fig. 7>**

We now discuss some of the plausible reasons for the observed discrepancies in wave attenuation.

#### 5.2.1 Linear constant viscoelasticity

The three theories considered are all based on linear viscoelastic assumptions. The dispersion relation in the WS model is based on treating the ice cover as a linear Voigt material with $G'$ independent of rotational frequency and $G''$ linearly varying with rotational frequency. In the SA model, the Euler-Bernoulli assumption is used with a linear complex modulus. When the ice thickness becomes very thin and the elastic modulus is sufficiently high, these two models essentially converge to each other (Mosig et al., 2015). The RP model (1990), though quite different from the above two, also assumes a linear combination of the elastic and viscous stresses.

For a strict linear Voigt model, the storage modulus $G'$ is constant with respect to varying frequency $\omega$, while $G''$ is linearly proportional to $\omega$, implying a constant viscosity with respect to $\omega$. Table 1 shows that our PDMS material is not strictly a linear Voigt material. We re-examine the SA and WS models and find that for a small amplitude monochromatic wave field, it is inconsequential whether the material is a linear Voigt material or frequency-dependent material. The same conclusion was also made in Mei et al. (2010) for wave-mud interactions. This is because each test involves a single frequency with the associated viscosity, hence there is no change in the form of the dispersion relation. The results shown in Figs. 6 and 7 already adopt these frequency dependent viscosities.

To check whether a small amplitude wave assumption did apply, we tried several different wave amplitudes in the experiments, the results are shown in Table 3. Under different wave amplitudes, the variation of the attenuation is much lower than the discrepancies observed in Fig 7. Thus, the observed discrepancy cannot be attributed to the material properties of the PDMS covers or the linearity of the experimental regime.

The data analysis and theoretical assumptions are thus both ruled out as the cause of the significant discrepancies observed between the experimental data and theoretical predictions. The extra mechanisms on attenuation that could be present in the experiments but not in the theories are analyzed next.

### 5.2.2 Damping due to water and wave flume interaction

It is known that in wave flumes, even under open water, there are several mechanisms that could produce damping (Miles, 1967). These mechanisms include: viscous dissipation between the water with rigid boundaries (walls and bottom), at the top surface, and the meniscus effect at the wall-air-water interface. For the top surface, minute impurities (surfactant or other films) could increase the wave damping from the clean water condition. Theoretical models were developed to account for these energy losses (Henderson et al., 2015). Using $\nu_w = 1.1 \times 10^{-6}$ m$^2$/s as the kinematic viscosity of clean water, the attenuation from (a) the wave surface is $\alpha_{CL} = \frac{2\nu_w k^2}{c_g} = \sim 0.001$ m$^{-1}$ and (b) the boundaries of the flume is $\alpha_{SB} = \sqrt{\frac{\omega\nu_w}{2}}\frac{k}{c_g}\left(\frac{1}{\sinh(2kd)} + \frac{1}{kB}\right) = 0.002$ m$^{-1}$ for $T = 0.5$ s, where $c_g$ is the group celerity (Sutherland et al., 2017). Both are two orders of magnitude lower than the discrepancies observed in Fig. 7. In the extreme case, the maximum dissipation due to the presence of massless floating film at the water surface $\sqrt{2}\left[\frac{\nu_w{}^2|k|^7}{g}\right]^{1/4} \approx 0.08$ m$^{-1}$ for T = 0.5 s (Henderson et al. 2015). This compares well to the maximum attenuation, $\alpha_o = 0.05$ m$^{-1}$ in open water, performed in our experiments (see Fig. 8). All these values due to the various mechanisms are therefore much too small to explain the discrepancies observed in Fig. 7.

### 5.2.3 Boundary effects due to the moving cover and side walls

Between the PDMS cover and the glass walls there is an allowance, $\Delta \cong 0.005$m, on both sides. The attenuation coefficient due to the side wall may be obtained by considering the viscous

dissipation per unit time per unit length caused by the fixed side wall on either side of the cover, $\frac{1}{T}$ $\int_o^T 2\nu_w\left(\frac{\partial u}{\partial y}\right)^2 dt \sim \frac{2\nu_w L_s\, t_s}{\Delta}\left(2\frac{\pi a}{T}\right)^2$. The corresponding energy dissipation per unit time per unit length is then $L_s\frac{d}{dx}(E_w c_g) \sim L_s\frac{a^2\alpha e^{-2\alpha L_s}\rho_w g}{T}\frac{\lambda}{2T}$, where $\lambda$ is the wavelength, $u$ is the horizontal orbital velocity, $E_w$ is the wave energy density, $\rho_w$ is density of water and $L_s$ is length of the covers. The corresponding coefficient $\alpha$ calculated for $T$ = 0.5 s is $10^{-6}$ $m^{-1}$, which is three orders of magnitude lower than all other mechanisms. In other words, the boundary effects due to the moving covers and the side walls are insignificant.

### 5.2.4 Boundary layer under the covers

For wave attenuation under ice covers, Weber (1987) and Liu and Mollo-Christensen (1988) considered the damping mechanisms in the water body below the ice cover. They used an eddy-viscosity to describe the boundary layer dynamics and the associated attenuation rate. The effect of a boundary layer beneath the viscoelastic covers was not considered in the three viscoelastic models. Here we first consider the laminar Stokes boundary layer (BL) theory which is only applicable to a rigid plate oscillating in a fluid. The viscous boundary layer for this situation has a thickness $\delta_s = 2\pi\sqrt{\frac{2\nu_w}{\sigma}}$. Using the kinematic viscosity and the wave frequencies in our study, this thickness is in the range of 0.0025 m to 0.0035 m for $T$ = 0.5 s to 1.0 s which is very small. Hence the attenuation coefficient from this boundary effect, $\frac{\pi\nu_w k}{\delta_s c_g} < O(10^{-2})$, is at least one order below the measured attenuation. The PVC cover tests shows significantly higher dissipation, as shown in Fig. 5(d) and Fig. 8 (circles) thus, the BL structure underneath the PVC covers is likely to be

turbulent. Without direct measurements of the flow structure under the PDMS viscoelastic covers, we can only speculate that for the PDMS covers the dissipation due to this boundary layer effect is also significant.

Sutherland et al. (2017) provided another estimate of the wave attenuation from the laminar boundary layer effect. For a floating but inextensible thin film (with modulus $E \to \infty$), the theoretical attenuation coefficient is given by $\alpha_{IN} = \frac{1}{2} \nu_w \gamma_a k / c_g$ where $\gamma_a = \sqrt{\frac{\sigma}{2\nu_w}}$. If a finite elasticity is considered, Christensen (2005) showed $\alpha_e = \alpha_{IN} \left[ \frac{2\varepsilon^2 + 4\,{}^{k}/_{\gamma_a}(1-\varepsilon)}{(1 - 2\varepsilon + 2\varepsilon^2)} \right]$ where $\varepsilon = \frac{E k^2 \gamma_a}{\rho_w \sigma^2}$.

For the present experiments with PVC film ($E \approx 1$ GPa), both formulas yield approximately the same value for the range of wave periods considered here. This boundary layer attenuation, $\alpha_{IN}$, is shown as the solid line in Fig. 8.

The estimated boundary layer attenuation in the present study, $\alpha_{IN}$, is much larger than the sum of theoretical predictions for clean water attenuation and side boundaries, $\alpha_{CL} + \alpha_{SB}$, hence the latter may be ignored from further analysis. Fig. 8 shows the measured PVC attenuation, calculated PVC attenuation using the inextensible assumption discussed above, and measured open water attenuation (from different wave amplitudes). The measured attenuation from the water body under the film is on the same order as the measured attenuation under the PDMS, which is not considered in the SA and WS models, but could be parameterized by RP model.

Notable discrepancy between $\alpha_{IN}$ and attenuation caused by PVC cover is evident in Fig 8. Quantitative discrepancies from 20% to 90% for higher frequencies were observed in the results by Sutherland et al (2017) when they tested very thin (0.25 to 0.5 mm) polypropylene and latex covers as well. A comparable discrepancy of almost twice the value of $\alpha_{IN}$ was observed for experiments conducted by Henderson et al. (2015) using floating cling wrap. The increased attenuation could be contributed by resonance effect due to the energy transfer from transverse to longitudinal waves when $\sigma = \left(\frac{2\nu\rho^2 g^4}{E^2}\right)^{\frac{1}{5}}$ (Sutherland et al., 2017). In this case, the resonant frequency is approximately 0.002 rad/s, which is 3 - 4 orders smaller than the experimental frequency range here, hence resonant effect can be ignored.

**< Fig. 8>**

The attenuation measured from the PVC film strongly suggests that the damping in the boundary layer is much more significant than what is anticipated from an oscillatory laminar boundary layer. From physical arguments, the no-slip condition generates flows that are determined by the boundary geometry and its dynamics. The cover changes the horizontal velocity from being max (free surface) to zero (if the cover is held in place with only one degree of freedom: vertical), which creates strong shear and damping in the BL. For the infinitely deep viscous model viscous model, the Reynolds number = $\frac{g^2}{4\nu\sigma^2}$ is $\sim O(10^5)$ with $\nu = 10^{-6}$ m$^2$/s for pure water for the wave parameters considered in the present study (Newyear and Martin, 1997). Adopting a Reynolds number in the form of $u_{max} * \delta/\nu$, where $\delta$ is the boundary layer thickness, previous research (e.g. Song and Law, 2015) had shown that the laminar boundary layer will transit to partial turbulence when Re > ~150 and fully developed turbulence when Re > ~500 for a fixed boundary. The corresponding energy

502 dissipation in the oscillatory turbulent BL would be much higher than that of the laminar BL.
503 However, how the undulating water surface interacts with the BL such that the critical Re may be
504 reduced to the range in our experiments, is not currently well understood and needs to be further
505 studied. This is a difficult hydrodynamic problem, we imagine, since even in open water, how
506 waves interact with the flow structure under the free surface is not completely known. Hence the
507 attenuation due to this effect would be unique for each cover and the wave period combination
508 considered. Without complete knowledge of this boundary layer structure, we could only estimate
509 its effect on wave attenuation as follow.

510

511 In Fig. 9, a rough estimate of the reduced attenuation due to PDMS covers is provided. The reduced
512 experimental attenuation coefficient for PDMS covers is obtained by subtracting the attenuation
513 due to the boundary layer effect using the PVC cover from the actual attenuation obtained for the
514 PDMS covers. The underlying assumption is that for the same wave period, the boundary
515 attenuation under the PDMS is the same as under the PVC cover. An improved correlation between
516 the reduced attenuation and theoretical predictions is obtained, as compared to Fig. 7.

517 **<Fig. 9>**

518 Finally, as discussed above, although the comparison for wavenumbers is quite good for thin
519 PDMS covers as shown in Fig. 7, it deteriorates for the thicker PDMS cover. We do not believe
520 that it is due to the edge effect since the extra wave mode existing near the leading edge is two
521 orders larger than the surface gravity waves with an attenuation rate = 25 $m^{-1}$. One possibility for
522 the discrepancy is that for a thicker cover the BL effect may begin to not only influence the
523 attenuation, but also the wave speed.

## 6. Conclusions

Floating viscoelastic covers with properties close to a linear Voigt material are prepared from oil-doped PDMS. Four different PDMS are tested that cover a range of shear modulus between 22 to 145 kPa, and viscosity between 0.23 to 0.67 $m^2/s$. Two different cover thickness, 0.01 and 0.02 m are also tested in this study. The wavenumber and attenuation along the covers are measured and compared with three different linear viscoelastic theories (Squire and Allan, 1980; Robinson and Palmer, 1990; and Wang and Shen, 2010).

Wave experiments show that the wavelength could be shorter or longer than the open water case, depending on wave period, material property and cover thickness. The theoretical predictions match reasonably well with the experiment results for larger periods and the thinner cover, while, some discrepancies are observed for the thicker cover.

The wave attenuation has large discrepancies between the theoretical predictions and experimental data, more so for shorter periods and the thicker cover. The effects due to several missing mechanisms that could be estimated based on fundamental knowledge in fluid mechanics are examined. The strongest effect appears to be the boundary layer below the flexing floating covers. The experiments with the PVC film confirm this conjecture. We note that similar effects are also expected in the field under real ice covers. As shown in recent studies (Smith et al., 2016; Marchenko et al., 2017), waves may create quite complicated flow structures under an ice cover.

546 Overall, the current findings highlight that a detailed study on the presence of boundary layer
547 underneath an oscillating cover, with its influence on decay of wave as well as wavenumber
548 modification, need to be performed in the future.

549

550 **Acknowledgments**

551

552 The authors gratefully acknowledge the funding provided by Ministry of Education, Singapore
553 through the AcRF Tier 2 Grant No. MOE2013-T2-1-054. This work is supported in part by the US
554 Office of Naval Research Grant #N00014-13-1- 0294 and US Office of Naval Research Global
555 Grant No: N62909-15-1-2069. The authors would like to thank Ms. Teo Wan Lin Jane, Ms. Neo
556 Ying Xue and Dr. Sourav Mandal for conducting the wave experiments and Dr Sukun Cheng for
557 supplying the code to select the gravity wave mode in the WS model.

558

559 **Appendix A:**

560

561 The positioning of ultrasound sensors over the 0.01 m thick covers is as follows:

562 (i) The first ultrasound sensor, US1, is fixed at 20 cm from the leading edge.

563 (ii) The second ultrasound sensor, US2, is placed at 50 cm from the leading edge and the other five
564 sensors are kept at 40 cm distance apart from each other following US2 towards the beach.

565 (iii) The first set of experiments are conducted with the position of the ultrasound sensors as
566 mentioned above for the required wave periods.

(iv) The second set of experiments are conducted after moving the ultrasound sensors other than US1 by 20 cm towards the beach from their previous position. Each experiment from the second set is also repeated three times. Because of the repeatability of the experiments, the two sets under the same wave condition are then combined to effectively increase the monitoring density along the floating covers. In all, each wave test is monitored at 13 locations with respective distance from the leading edge as: 20, 50, 70, 90, until 270 cm.

For the 0.02 m thick PDMS cover, the distance between the sensors is maintained at 20 cm for the first set of experiments. In the second set of experiments, all the sensors are shifted by 10 cm from their previous position (except US1), resulting in the 13 locations as: 20, 50, 60, 70, until 160 cm. This positioning is done so that the surface elevation under stronger attenuation is still within the measurable range of the ultrasound sensors.

For each PDMS cover, the time series of surface displacement data at 13 locations along the length of the cover are obtained with a total of 66 experiments (i.e. 11 wave periods × 2 position changes × 3 repetitions). Open water experiments and experiments with floating PVC film are also conducted with the same input wave conditions to compare with the viscoelastic floating cover cases.

For each PVC cover, the time series of surface displacement data at only 7 locations along the length of the cover are obtained with no shift provided for the sensors. Thus, a total of 33 experiments (i.e. 11 wave periods × 1 position × 3 repetitions) are conducted. Open water

589 experiments and experiments with floating PVC film are also conducted with the same input wave
590 conditions to compare with the viscoelastic floating cover cases.

591

592 **Appendix B**

593

594 The procedure for data analysis is validated using open water condition, where the measured wave
595 speed is confirmed with the theoretical value. For covered case, we repeated each test at least three
596 times with almost identical results. Reflection from the beach is carefully removed, with details
597 given below.

598

599 One common challenge in a wave flume facility, to analyze wave parameters, is to avoid
600 contamination from the beach reflection. Reflection can produce a partial standing wave that can
601 influence both celerity and attenuation measurements. The only way to avoid the influence of
602 reflection is to truncate the data at the time before the arrival of the reflection, which may be
603 estimated using the wave celerity. Hence, the number of "clean waves" is first determined in the
604 data analysis. The time needed for the wave energy to travel from each sensor with the group
605 celerity, reflected from the vertical wall near the beach and return to the sensor is calculated. The
606 time taken for each wave to make a round trip from a sensor to the wall is denoted by $t_r$. This time
607 span is calculated as twice the distance between sensor location and wall ($x_b$) divided by $c_g$, $t_r =$
608 $2x_b/c_g$. The number of waves considered free from reflection is calculated as $N_c = \frac{t_r}{T} - N_d$, where
609 $N_d$ is the number of waves generated before the fully developed wave, which is estimated from the

610 ultrasound signal. Using this method, we found that for $T = 0.5$ s, $N_c$ was 33 for US1 and 8 for
611 US13. For $T = 1.0$ s, $N_c$ was 4 for the US1 and 3 for the US4. Since only three fully developed
612 waves are considered to obtain the wave attenuation throughout the analysis, the portion of the
613 PDMS covers where $N_c < 3$ are excluded from further analysis. Thus, the effect of reflection can
614 be ruled out as the reason for discrepancy between experimental data and theoretical results.

615

616 **REFERENCES**

617

618 Cheng, S., Rogers, W.E., Thomson, J., Smith, M., Doble, M., Wadhams, P., Kohout, A.L., Lund,
619 B., Persson, O., Collins, C.O., Ackley, S.F., Montiel, F., Shen, H.H., 2017. Calibrating a
620 viscoelastic sea ice model for wave propagation in the Arctic fall marginal ice zone. J. Geophys.
621 Res. Oceans. doi:10.1002/2017JC013275

622 Christensen, K.H., 2005. Transient and steady drift currents in waves damped by
623 surfactants. Physics of Fluids, 17(4), 042102.

624 Collins, C.O., Rogers, W.E., Lund, B., 2017. An investigation into the dispersion of ocean surface
625 waves in sea ice. Ocean Dynamics, 67(2), 263-280.

626 De Carolis, G., Desiderio, D., 2002. Dispersion and attenuation of gravity waves in ice: a two-
627 layer viscous fluid model with experimental data validation. Physics Letters A, 305(6), 399-412.

628 De Carolis, G., Olla, P., Pignagnoli, L., 2005. Effective viscosity of grease ice in linearized gravity
629 waves. J. Fluid Mech. 535, 369–381.

630 Folch, A., 2012. Introduction to BioMEMS. Bosa Roca: Taylor and Francis. pp 22–24.

631 Fox, C., Squire, V.A., 1990. Reflection and transmission characteristics at the edge of shore fast
632 sea ice. J. Geophys. Res.: Ocean (1978-2012), 95 (C7), 11629-11639.

633 Fox, C., Haskell, T. G., 2001. Ocean wave speed in the Antarctic marginal ice zone. Annals of
634 Glaciology, 33, 350-354.

635 Greenhill, A.G., 1886. Wave motion in hydrodynamics. American Journal of Mathematics, 62-96.

636 Henderson, D., Rajan, G.K., Segur, H., 2015. Dissipation of narrow-banded surface water waves.
637 In Hamiltonian Partial Differential Equations and Applications (pp. 163-183). Springer, New
638 York, NY.

639 Hermans, A.J., 2004. Interaction of free-surface waves with floating flexible strips. Journal of
640 engineering mathematics, 49(2), 133-147.

641 Keller, J.B., Weitz, M., 1953. Reflection and transmission coefficients for waves entering or
642 leaving an icefield. Communications on Pure and Applied Mathematics, 6(3), 415-417.

643 Keller, J.B., 1998. Gravity waves on ice-covered water. Journal of Geophysical Research:
644 Oceans, 103(C4), 7663-7669.

645 Kohout, A. L., Meylan, M. H., Plew, D. R., 2011. Wave attenuation in a marginal ice zone due to
646 the bottom roughness of ice floes. Annals of Glaciology, 52(57), 118-122.

647 Lamb, H., 1932. Hydrodynamics. Cambridge university press, pp 738.

648 Li, J., Mondal, S., Shen, H.H., 2015. Sensitivity analysis of a viscoelastic parameterization for
649 gravity wave dispersion in ice covered seas. Cold Regions Science and Technology, 120, 63-75.

650 Liu, A.K., Mollo-Christensen, E., 1988. Wave propagation in a solid ice pack. Journal of physical
651 oceanography, 18(11), 1702-1712.

652 Marchenko, A.V., Gorbatsky, V.V., Turnbull, I. D., 2015. Characteristics of under-ice ocean
653 currents measured during wave propagation events in the Barents Sea. In Proceedings of the
654 International Conference on Port and Ocean Engineering Under Arctic Conditions, Norway.

655 Mei, C.C., Krotov, M., Huang, Z., Huhe, A., 2010. Short and long waves over a muddy seabed. J.
656 Fluid Mech., 643, 33-58.

Meylan, M.H., Bennetts, L.G., Kohout, A.L., 2014. In situ measurements and analysis of ocean waves in the Antarctic marginal ice zone. Geophysical Research Letters, 41(14), 5046-5051.

Miles, J.W., 1967. Surface-wave damping in closed basins. Proceedings of the Royal Society of London A: Mathematical, Physical and Engineering Sciences, 297(1451), 459–475. DOI: 10.1098/rspa.1967.0081

Mosig, J.E., Montiel, F., Squire, V.A., 2015. Comparison of viscoelastic-type models for ocean wave attenuation in ice-covered seas. Journal of Geophysical Research: Oceans, 120(9), 6072-6090.

Newyear, K., Martin, S., 1997. A comparison of theory and laboratory measurements of wave propagation and attenuation in grease ice. Journal of Geophysical Research: Oceans, 102(C11), 25091-25099.

Newyear, K., Martin, S., 1999. Comparison of laboratory data with a viscous two-layer model of wave propagation in grease ice. Journal of Geophysical Research: Oceans, 104(C4), 7837-7840.

Peters, A.S., 1950. The effect of a floating mat on water waves. Communications on Pure and Appled Mathematics, 3(4), 319-354.

Robinson, N.J., Palmer, S.C., 1990. A modal analysis of a rectangular plate floating on an incompressible liquid. Journal of sound and Vibration, 142(3), 453-460.

Schulz-Stellenfleth, J., Lehner, S., 2002. Spaceborne synthetic aperture radar observations of ocean waves traveling into sea ice. Journal of Geophysical Research: Oceans, 107(C8), 20(1-19).

Smith, L.C., Stephenson, S.R., 2013. New Trans-Arctic shipping routes navigable by midcentury. Proceedings of the National Academy of Sciences,110(13), E1191-E1195.

678 Smith, M., Thomson, J.M., Stammerjohn, S.E., Persson, O.G., Rainville, L., 2016. Observations
679 of wave-enhanced mixing in the autumn Arctic Ocean, Poster C21C-0695, AGU Fall Meeting
680 2016, San Francisco, CA.

681 Song, J., Law, A.W.K. 2015. Longitudinal dispersion of turbulent oscillatory pipe flows.
682 Environmental Fluid Mechanics, 15(3), 563-593

683 Squire, V.A., Allan, A.J., 1980. Propagation of flexural gravity waves in sea ice, in Sea Ice
684 Processes and Models, Proceedings of the Arctic Ice Dynamics Joint Experiment, edited by R. S.
685 Pritchard, pp. 327–338, Univ. of Wash. Press, Seattle, Wash.

686 Squire, V.A., 1993. A comparison of the mass-loading and elastic plate models of an ice field. Cold
687 regions science and technology, 21(3), 219-229.

688 Sree, D.K., Law, A.W.K., Shen, H.H., 2016a. An experimental study on the interactions between
689 surface waves and floating viscoelastic covers. Wave Motion, 70, 195-208.

690 Sree, D.K., Law, A.W.K., Shen, H.H., 2016b. Attenuation of surface wave by viscoelastic floating
691 cover: An experimental study. 23rd IAHR International Symposium on Ice, Ann Arbor, *Michigan.*

692 Stokes, G. G., 1851. On the effect of the internal friction of fluids on the motion of pendulums.
693 Cambridge: Pitt Press, Vol. 9, p. 8.

694 Sutherland, G., Rabault, J., 2016. Observations of wave dispersion and attenuation in landfast
695 ice. Journal of Geophysical Research: Oceans, 121(3), 1984-1997

696 Sutherland, G., Halsne, T., Rabault, J., Jensen, A., 2017. The attenuation of monochromatic
697 surface waves due to the presence of an inextensible cover. Wave Motion, 68, 88-96.

698 Wadhams, P., Squire, V.A., Ewing, J.A., Pascal, R.W., 1986. The effect of the marginal ice zone
699 on the directional wave spectrum of the ocean. Journal of physical oceanography, 16(2), 358-376.

700 Wadhams, P., Squire, V.A., Goodman, D.J., Cowan, A.M., Moore, S.C., 1988. The attenuation
701 rates of ocean waves in the marginal ice zone. Journal of Geophysical Research: Oceans, 93(C6),
702 6799-6818.

703 Wadhams, P., Parmiggiani, F., De Carolis, G., 2002. The use of SAR to measure ocean wave
704 dispersion in frazil-pancake icefields. Journal of physical oceanography, 32(6), 1721-1746.

705 Wang, R., Shen, H.H., 2010. Gravity waves propagating into an ice-covered ocean: A viscoelastic
706 model. Journal of Geophysical Research: Oceans, 115(C6), C06024(1-12).

707 Weber, J. E., 1987. Wave attenuation and wave drift in the marginal ice zone. Journal of physical
708 oceanography, 17(12), 2351-2361.

709 Weitz, M., Keller, J.B., 1950. Reflection of water waves from floating ice in water of finite
710 depth. Communications on Pure and Applied Mathematics,3(3), 305-318.

711 Zhao, X., Shen, H.H., 2015. Wave propagation in frazil/pancake, pancake, and fragmented ice
712 covers. Cold Regions Science and Technology,113, 71-80.

713 Zhao, X., Cheng, S., Shen, H.H., 2017. Nature of wave modes in coupled viscoelastic layer over
714 water, J. Eng. Mech., 143(10): 04017114, doi:10.1061/(ASCE)EM.1943-7889.0001332.

715

716 **List of Tables**

717

718 **Table 1** Mechanical properties of PDMS cover. Viscosity and shear modulus obtained for Voigt

719 model.

720 **Table 2** Input wave characteristics.

721 **Table 3** Variation of wavelength and attenuation coefficient with wave amplitude. $m_{CA}$= 4%, $h_s$

722 = 0.02 m.

723

**List of Figures**

745 $\alpha_{IN}$), Black asterisk = experimental data for open water experiment for amplitude, $a$ = 0.01 m, and
746 Grey asterisk = experimental data for open water experiment with reduced wave amplitude as
747 mentioned in Table 2 for $h_s$= 0.01 m. In the experiment, each test was repeated at least three times.
748 The circles are the mean of each test and the error bars represent the 95% confidence interval limit
749 for fitted curve.

750 **Fig. 9.** Reduced attenuation coefficient against wave period ($h_s$ = 0.01 m). Triangle = reduced
751 experimental data, model predictions: a) Dark grey dotted line = SA model, and b) Light grey solid
752 line = WS model.

753

**List of Abbreviations**

| | |
|---|---|
| MIZ | Marginal Ice Zone |
| PDMS | Polydimethylsiloxane |
| PVC | Polyvinyl chloride |
| RP | Robinson and Palmer model (1990) |
| SA | Squire and Alan model (1980) |
| US | ultra sound |
| WS | Wang and Shen model (2010) |

**List of Symbols**

| | |
|---|---|
| $a$ | wave amplitude in open water |
| $B$ | breadth of wave flume |
| $c_o$ | open water wave celerity |
| $c_s$ | wave celerity under the floating cover |
| $c_g$ | group celerity of wave |
| $D$ | depth of wave flume |
| $d$ | water depth |
| $E_w$ | wave energy |
| $E$ | Young's modulus of elasticity |
| $g$ | acceleration due to gravity |
| $G$ | shear modulus |
| $G^{'}$ | storage modulus |
| $G^{''}$ | loss modulus |
| $G_V$ | complex Voigt shear modulus |
| $h$ | thickness of upper layer |
| $h_s$ | thickness of PDMS cover |

| | | |
|---|---|---|
| 782 | $H$ | thickness of lower layer |
| 783 | $k_o$ | wavenumber in open water |
| 784 | $k$ | complex wavenumber |
| 785 | $k_i$ | imaginary part of the complex wavenumber |
| 786 | $k_s$ | wavenumber under the floating cover / real part of complex wavenumber |
| 787 | $L$ | length of wave flume |
| 788 | $L_s$ | length of sheet |
| 789 | $M_B$ | mass of base |
| 790 | $m_{CA}$ | mass percentage of curing agent |
| 791 | $M_{CA}$ | mass of curing agent |
| 792 | $N_c$ | number of waves free from reflection |
| 793 | $N_d$ | number of transient waves |
| 794 | $T$ | wave period |
| 795 | $u$ | horizontal orbital velocity of wave |
| 796 | $\omega$ | angular frequency of rheometer |
| 797 | $\sigma$ | wave frequency |
| 798 | $\eta$ | surface displacement |
| 799 | $A_x$ | amplitude along the cover at $x$ |

| | | |
|---|---|---|
| 800 | $A_o$ | amplitude along the cover at $x = 0$ |
| 801 | $\alpha_o$ | attenuation coefficient for open water condition |
| 802 | $\alpha$ | experimentally determined attenuation coefficient |
| 803 | $\vartheta$ | Poisson's ratio |
| 804 | $\rho_1$ | density of upper layer |
| 805 | $\rho_2$ | density of lower layer |
| 806 | $\rho_w$ | density of water |
| 807 | $\nu_e$ | complex viscosity |
| 808 | $\nu$ | real part of complex viscosity |
| 809 | $\nu_w$ | viscosity of water |
| 810 | $\kappa$ | normalized wavenumber, $k_s/k_o$ |
| 811 | $\delta_s$ | Stokes boundary layer thickness |
| 812 | $\lambda$ | wavelength |
| 813 | $\Delta$ | gap between PDMS cover and side wall |
| 814 | $\gamma$ | viscous term in RP model |
| 815 | $\alpha_{IN}$ | attenuation due to inextensible film |
| 816 | $\alpha_{CL}$ | clean water attenuation |
| 817 | $\alpha_{SB}$ | attenuation due to flume boundaries |

818 $\alpha_e$ attenuation due to floating cover of finite elasticity and negligible thickness

819

820

821

822

**Fig. 1.** Curing of PDMS inside wave flume (view from above).

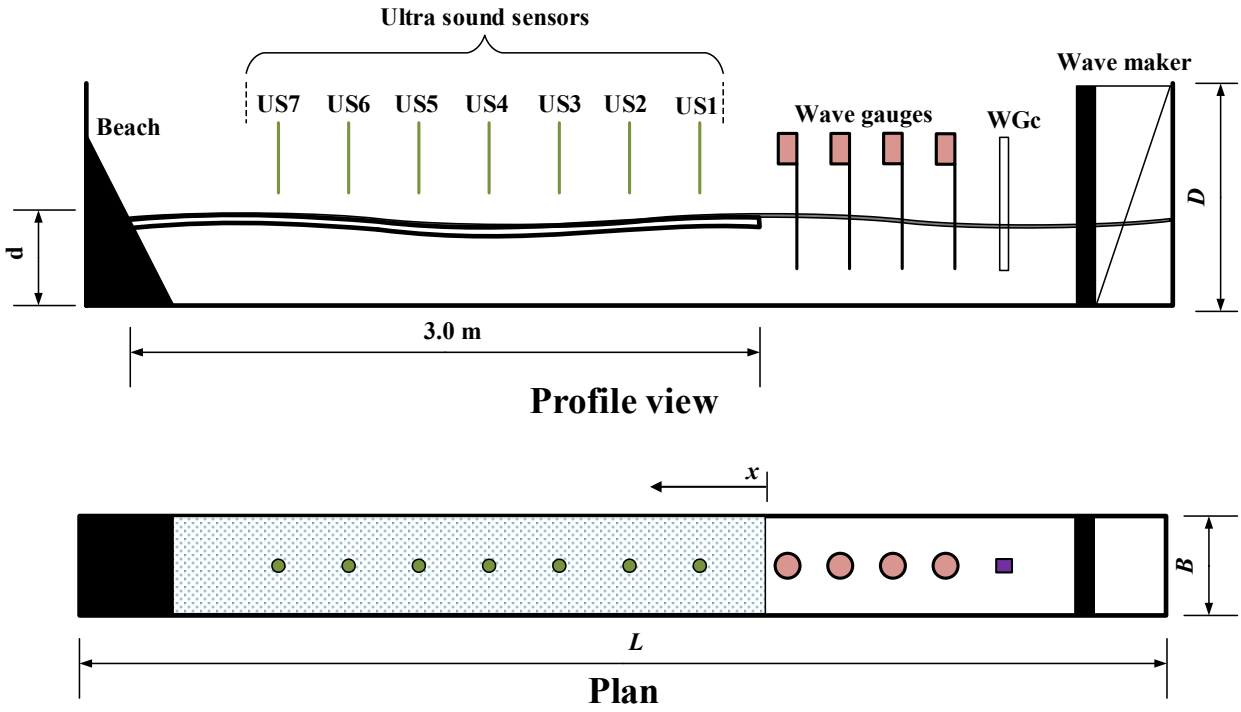


4

5 **Fig. 2.** Schematic diagram of wave flume.

6

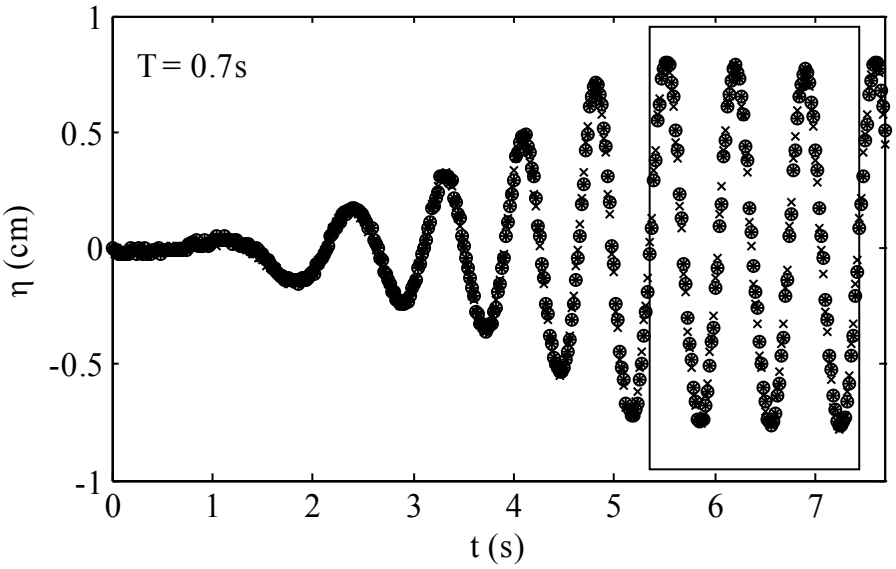


**Fig. 3.** The surface profile data obtained using US1 for $T$ = 0.7 s, $m_{CA}$ = 4% and cover thickness, $h_s$ = 0.01 m. The three fully developed waves considered are enclosed in the rectangle box, the repeatability of test is confirmed using three experiments (cross symbol, asterisk and circle).

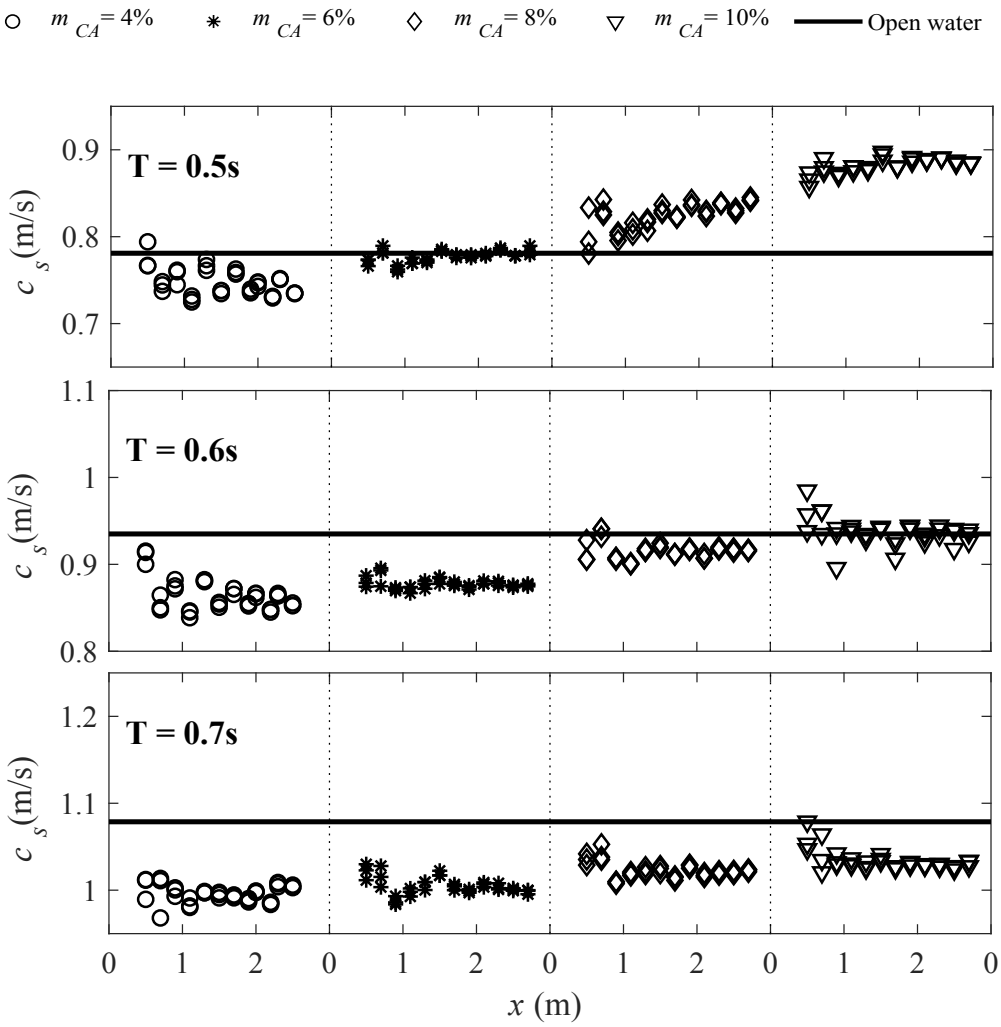


**Fig. 4.** Wave celerity along the length of the PDMS cover, $h_s$ = 0.01 m. To aid visualization, figure for each wave period is separated by dotted lines into 4 plots for different values of $m_{CA}$: Circles = 4%, asterisk = 6%, diamonds = 8%, and triangle = 10%. Solid line = open water wave velocity.

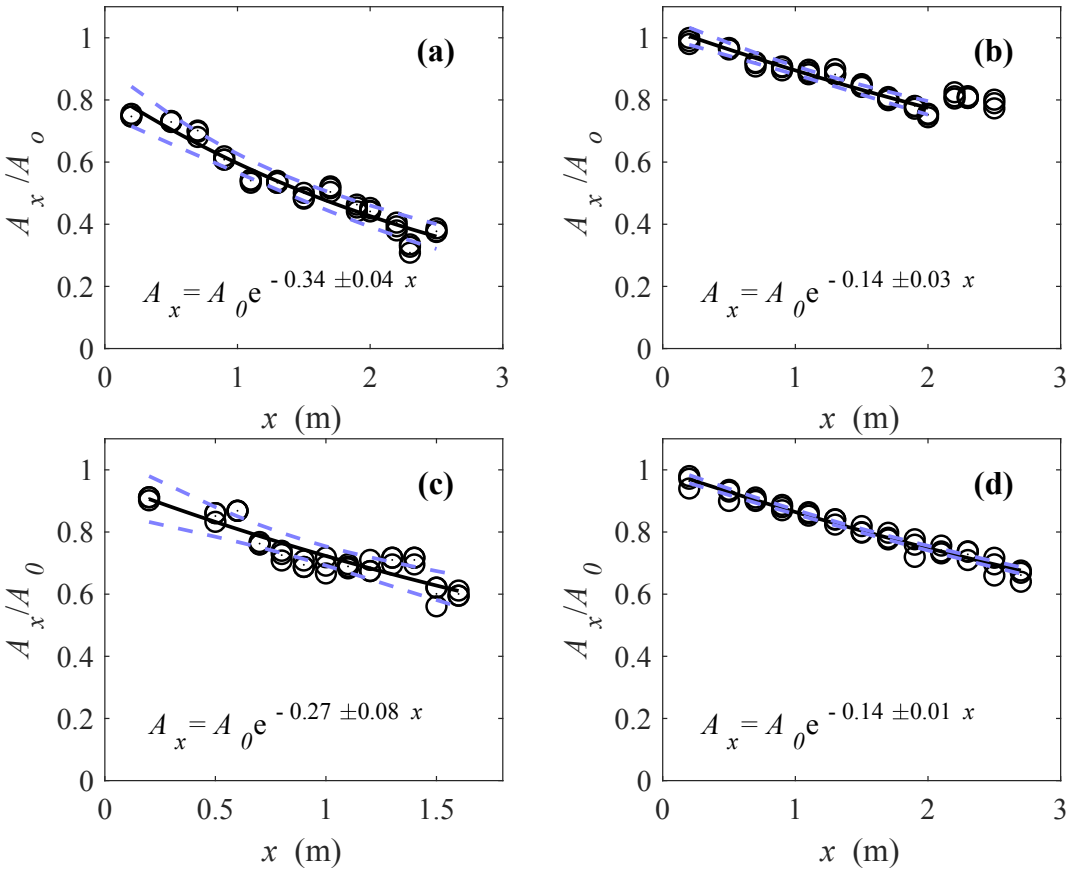


**Fig. 5.** Normalized wave amplitude along the length of the floating covers. PDMS cover with $m_{CA}$ = 4%, $h_s$ = 0.01 m and $T$ = a) 0.5 s and b) 0.7s. Wave attenuation along: c) PDMS cover with $m_{CA}$ = 4%, $h_s$ = 0.02 m and $T$ = 0.5 s, and d) PVC film for $T$ = 0.5 s. Overlapping circles confirms the repeatability of tests. The solid line indicates the exponential fit curve and dashed line indicates the 95% simultaneous functional prediction bounds of the fitted curve.

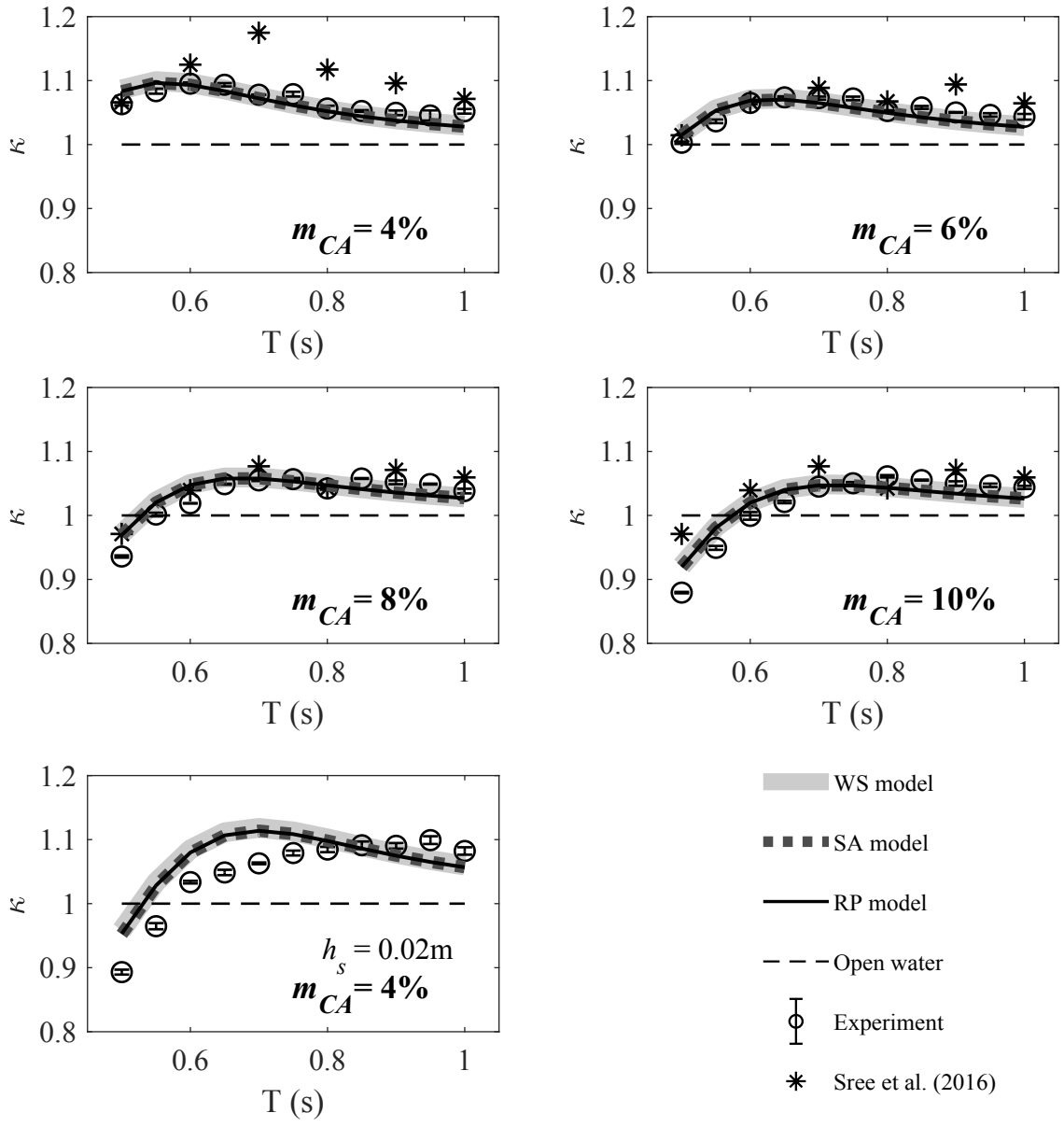


27

28

29

30 **Fig. 6.** Variation in normalized wavenumber with wave period for PDMS cover ($h_s$ = 0.01 m). The

31 three model predictions are practically identical.

32

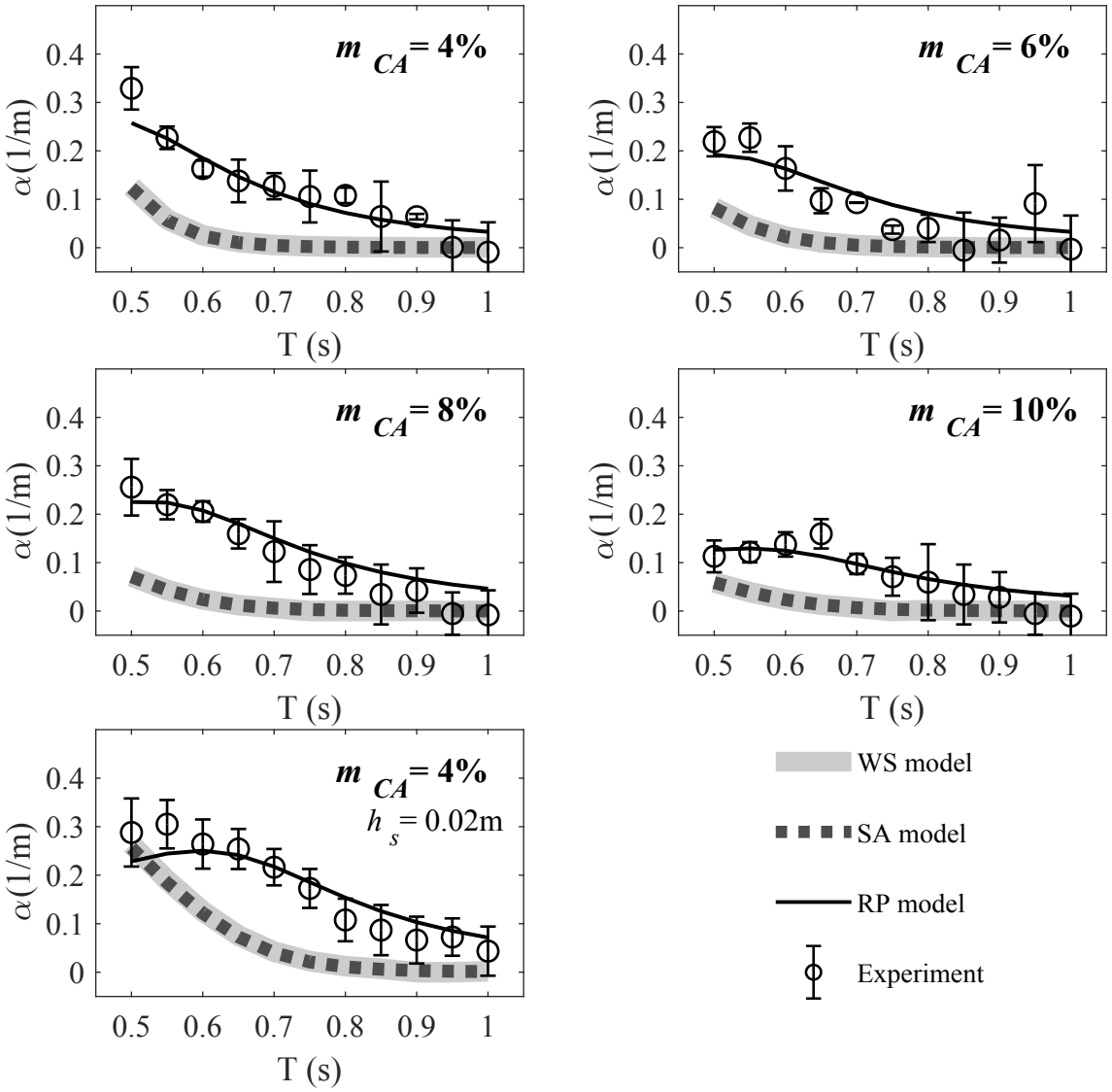


**Fig. 7.** Attenuation coefficient against wave period ($h_s$ = 0.01 m). The circles are the mean of each test and the error bars represent the 95% confidence interval limit for fitted curve.

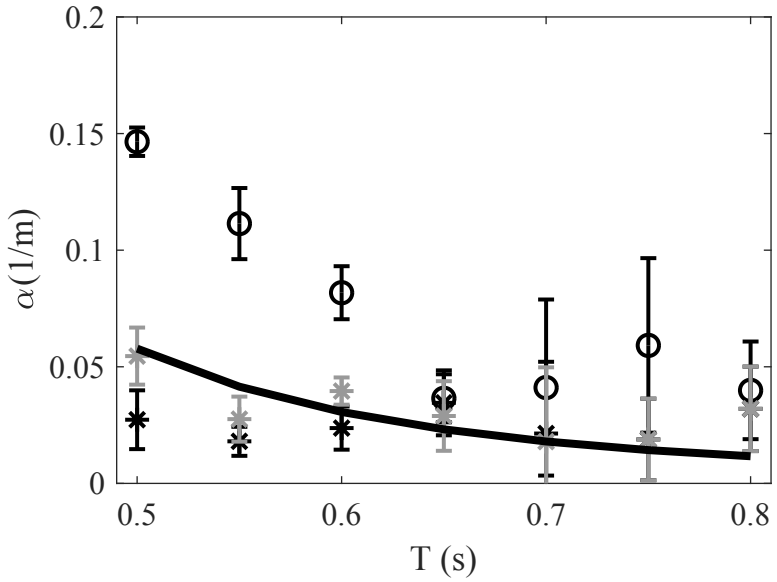


**Fig. 8**. Wave attenuation due to all additional damping mechanisms. Circles = experimental data for PVC cover, Black solid line = theoretically obtained attenuation due to inextensible sheet ( $\alpha_{IN}$), Black asterisk = experimental data for open water experiment for amplitude, $a$ = 0.01 m, and Grey asterisk = experimental data for open water experiment with reduced wave amplitude as mentioned in Table 2 for $h_s$= 0.01 m. In the experiment, each test was repeated at least three times. The circles are the mean of each test and the error bars represent the 95% confidence interval limit for fitted curve.

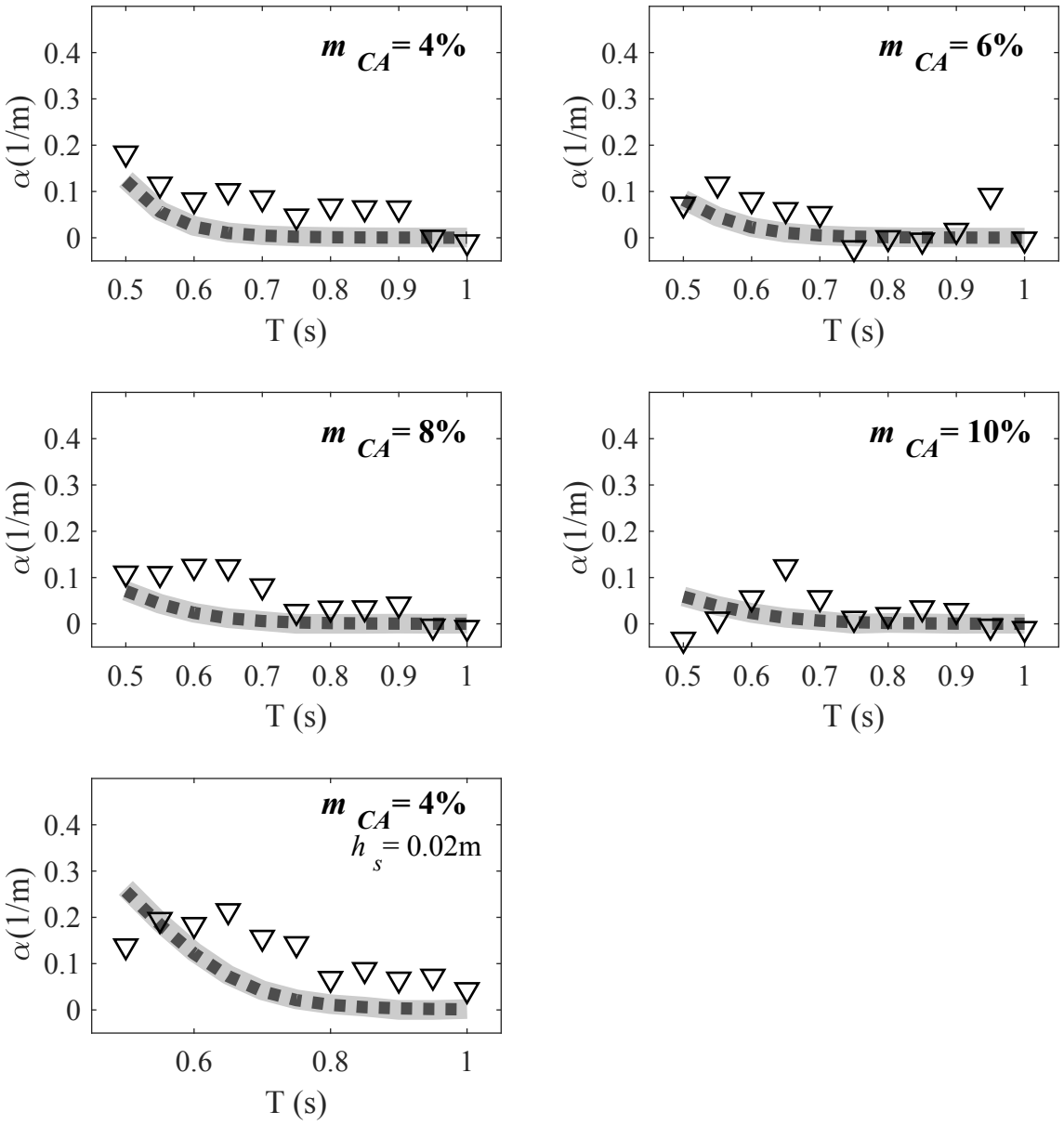


**Fig. 9.** Reduced attenuation coefficient against wave period ($h_s$ = 0.01 m). Triangle = reduced experimental data, model predictions: a) Dark grey dotted line = SA model, and b) Light grey solid line = WS model.

**Table 1**

Mechanical properties of PDMS cover. Viscosity and shear modulus obtained for Voigt model.

| $T$ (s) | $\omega$ (rad/s) | $G''$(kPa) | | | | $G' = G$ (kPa) | | | | $\nu = G''/\rho\omega$ (m$^2$/s) | | | |
|---|---|---|---|---|---|---|---|---|---|---|---|---|---|
| | | 4% | 6% | 8% | 10% | 4% | 6% | 8% | 10% | 4% | 6% | 8% | 10% |
| 0.50 | 12.56 | 2.70 | 3.12 | 3.92 | 4.92 | 23.18 | 55.64 | 89.79 | 145.11 | 0.23 | 0.26 | 0.33 | 0.42 |
| 0.55 | 11.42 | 2.61 | 3.02 | 3.81 | 4.77 | 23.06 | 55.47 | 89.60 | 144.91 | 0.24 | 0.28 | 0.35 | 0.44 |
| 0.60 | 10.47 | 2.53 | 2.9 | 3.71 | 4.64 | 22.95 | 55.33 | 89.45 | 144.75 | 0.26 | 0.30 | 0.38 | 0.47 |
| 0.65 | 9.67 | 2.45 | 2.863 | 3.62 | 4.53 | 22.85 | 55.21 | 89.29 | 144.58 | 0.27 | 0.32 | 0.40 | 0.50 |
| 0.70 | 8.98 | 2.37 | 2.79 | 3.53 | 4.40 | 22.73 | 55.10 | 89.15 | 144.39 | 0.28 | 0.33 | 0.42 | 0.52 |
| 0.75 | 8.38 | 2.31 | 2.72 | 3.45 | 4.30 | 22.64 | 55.00 | 89.02 | 144.23 | 0.29 | 0.35 | 0.44 | 0.55 |
| 0.80 | 7.85 | 2.25 | 2.66 | 3.37 | 4.21 | 22.55 | 54.92 | 88.90 | 144.09 | 0.30 | 0.36 | 0.46 | 0.57 |
| 0.85 | 7.39 | 2.19 | 2.61 | 3.31 | 4.13 | 22.48 | 54.84 | 88.80 | 143.96 | 0.32 | 0.38 | 0.48 | 0.59 |
| 0.90 | 6.98 | 2.15 | 2.56 | 3.26 | 4.05 | 22.41 | 54.78 | 88.71 | 143.85 | 0.33 | 0.39 | 0.50 | 0.62 |
| 0.95 | 6.61 | 2.11 | 2.52 | 3.21 | 3.99 | 22.35 | 54.72 | 88.63 | 143.75 | 0.34 | 0.41 | 0.52 | 0.64 |
| 1.00 | 6.28 | 2.07 | 2.48 | 3.16 | 3.93 | 22.30 | 54.66 | 88.56 | 143.66 | 0.35 | 0.42 | 0.54 | 0.67 |

**Table 2**

Input wave characteristics.

| $T$ (s) | $\lambda$ (m) | $k_o$ (rad/m) | $a \times 10^{-2}$(m) | $k_o a$ | $h_s$ (m) |
|---|---|---|---|---|---|
| 0.50 | 0.39 | 16.20 | 0.43 | 0.07 | 0.02 |
| | | | 0.51 | 0.08 | 0.01, 0.02 |
| 0.55 | 0.47 | 13.32 | 0.43 | 0.06 | 0.02 |
| | | | 0.51 | 0.07 | 0.02 |
| | | | 0.60 | 0.08 | 0.01, 0.02 |
| 0.60 | 0.56 | 11.24 | 0.51 | 0.06 | 0.02 |
| | | | 0.60 | 0.07 | 0.02 |
| | | | 0.68 | 0.08 | 0.01, 0.02 |
| 0.65 | 0.65 | 9.72 | 0.72 | 0.07 | 0.02 |
| | | | 0.85 | 0.08 | 0.01, 0.02 |
| 0.70 | 0.76 | 8.29 | 0.85 | 0.07 | 0.01, 0.02 |
| 0.75 | 0.86 | 7.31 | 0.85 | 0.06 | 0.01, 0.02 |
| 0.80 | 0.96 | 6.56 | 0.85 | 0.06 | 0.01, 0.02 |
| 0.85 | 1.05 | 5.99 | 0.85 | 0.05 | 0.01, 0.02 |
| 0.90 | 1.14 | 5.50 | 0.85 | 0.05 | 0.01, 0.02 |
| 0.95 | 1.26 | 4.99 | 0.85 | 0.04 | 0.01, 0.02 |
| 1.00 | 1.37 | 5.57 | 0.85 | 0.04 | 0.01, 0.02 |

**Table 3**

Variation of wavelength and attenuation coefficient with wave amplitude. $m_{CA}$= 4%, $h_s$= 0.02 m.

| $a \times 10^{-2}$ (m) | | 0.43 | 0.51 | 0.60 | 0.68 | 0.73 | 0.85 | 0.43 | 0.51 | 0.60 | 0.68 | 0.73 | 0.85 |
|---|---|---|---|---|---|---|---|---|---|---|---|---|---|
| | | $\kappa$ (mean $\pm$ standard deviation) | | | | | | $\alpha$ (1/m) mean (lower upper, limit of 90% confidence interval) | | | | | |
| $T$(s) | 0.50 | 0.89 $\pm$ 0.02 | 0.89 $\pm$ 0.02 | - | - | - | - | 0.28 (0.22,0.36) | 0.27 (0.19,0.35) | - | - | - | - |
| | 0.55 | 0.96 $\pm$ 0.01 | 0.96 $\pm$ 0.01 | 0.97 $\pm$ 0.02 | - | - | - | 0.30 (0.25,0.36) | 0.24 (0.18,0.30) | 0.22 (0.15,0.28) | - | - | - |
| | 0.60 | - | 1.03 $\pm$ 0.01 | 1.03 $\pm$ 0.01 | 1.04 $\pm$ 0.02 | - | - | - | 0.22 (0.16,0.27) | 0.26 (0.21,0.31) | 0.26 (0.21,0.30) | - | - |
| | 0.65 | - | - | - | - | 1.05 $\pm$ 0.03 | 1.07 $\pm$ 0.02 | - | - | - | - | 0.25 (0.21,0.29) | 0.25 (0.22,0.28) |